Electronic Supplementary Material (ESI) for Journal of Materials Chemistry C.

Supporting Information

Designed hollow Ni_2P/TiO_2 S-scheme heterojunction for remarkably enhanced photoelectric effect for solar energy harvesting and conversion

Youbo Nan [a,c], Xiutong Wang [a,b,c,d*], Shaohua Xing [e], Hui Xu [a], Jianmin Niu [f], Meipeng Ren [g],Teng Yu [a], Yanliang Huang [a], Baorong Hou [a]

[a] Key Laboratory of Marine Environmental Corrosion and Bio-fouling, Institute of Oceanology, Chinese Academy of Sciences, Qingdao, 266071, China

[b] Open Studio for Marine Corrosion and Protection, Pilot National Laboratory for Marine Science and Technology, Qingdao, 266237, China

[c] University of Chinese Academy of Sciences, Beijing 100049, China

[d] Center for Ocean Mega-Science, Chinese Academy of Sciences, Qingdao, 266071, China

[e] State Key Laboratory for Marine Corrosion and Protection, Luoyang ship material research institute, Qingdao 266237, China

[f] Shanghai Shipbuilding Technology Research Institute, Shanghai 200032, China

[g] CNOOC Research Institute Ltd., Beijing 100028, China

Density functional theory calculations

The Vienna Ab Initio Package (VASP)[1, 2] was employed to perform all the density functional theory (DFT) calculations within the generalized gradient approximation (GGA) using the PBE[3]formulation. The projected augmented wave (PAW) potentials [4, 5] to describe the ionic cores and take valence electrons into account using a plane wave basis set with a kinetic energy cutoff of

400 eV. Partial occupancies of the Kohn−Sham orbitals were allowed using the Gaussian smearing method and a width of 0.05 eV. The electronic energy was considered self-consistent when the energy change was smaller than 10^{-4} eV. The Ni_2P (111) surface had been obtained from the Ni_2P bulk structures with the lattice parameters (a=13.5214Å, b=6.7607Å, c=23.520Å). And the four-layers had been chosen in the Ni_2P (111) surface. In addition, the TiO_2(101) surface had been obtained from the supercell TiO_2 bulk structures with the lattice parameters (a=10.4632Å, b=7.6054Å, c=27.971Å). The Ni_2P/TiO_2 structures had been established using the Ni_2P (111) surface and TiO_2(101) surface with 10-layers. Finally, the optimized lattice parameters is a=11.9923Å, b=7.1831Å, c=36.5191Å. And interface Mismatch is less than 10%. A geometry optimization was considered convergent when the force change was smaller than 0.04 eV/Å. During structural optimizations, the 2×2×1 Monkhorst-Pack k-point grid for Brillouin zone was used for k-point sampling, and all atoms were allowed to relax. In addition, the U correction had been set as 3.69 eV and 4.25 eV for Ni and Ti atoms in our systems.

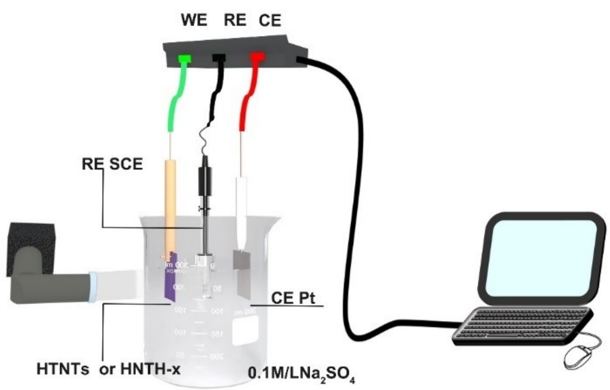

Fig. S1 Schematic diagram of the i-V and EIS curve test device

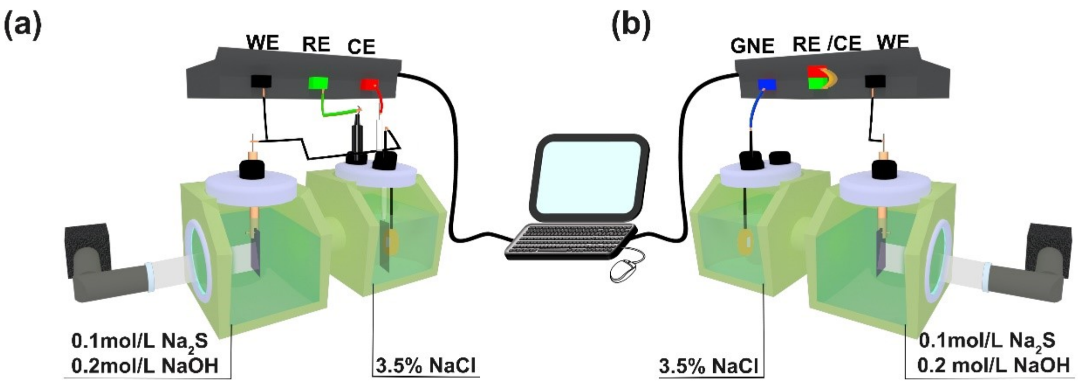

Fig. S2 Schematic diagram of the photoelectric chemical test device: (a) OCP and (b) j-t

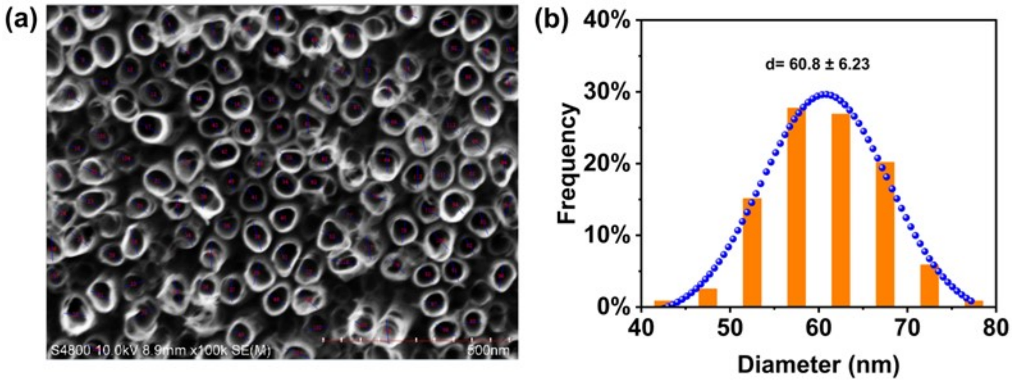

Fig. S3 The pore size distribution of TiO_2 nanotubes

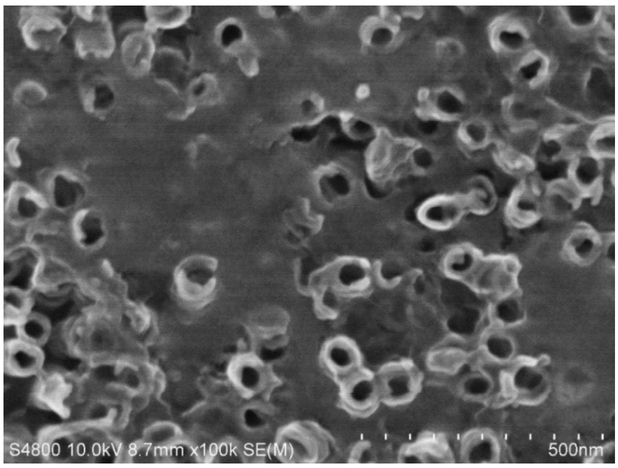

Fig. S4 Top-view SEM images of Ni_2P/TiO_2 -30

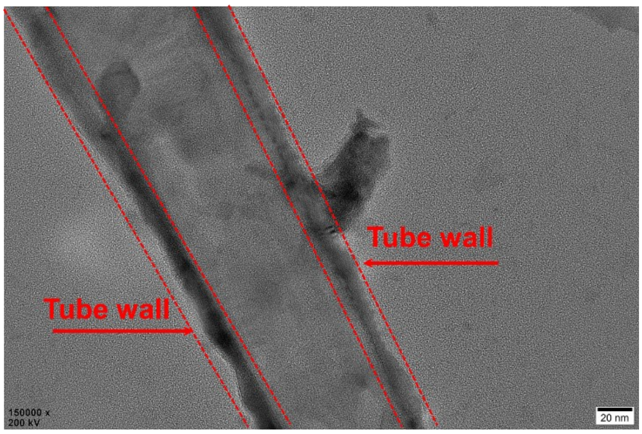

Fig. S5 (a-e) TEM image of single Ni_2P/TiO_2-15 nanotube

Note S1: TEM image of Ni_2P/TiO_2-15 and its elemental mapping

To explore the distribution of Ni_2P on the surface of the TiO_2 NTs and the inner wall of the tube, a transmission electron microscope line scan was used to characterize the types and contents of elements at various points in a certain line of sample Ni_2P/TiO_2-15. In addition, the distribution state of the tubular structural elements of the prepared sample was characterized by means of a mapping scan. Fig. S6 (a-e) shows the TEM image of Ni_2P/TiO_2-15 and the corresponding surface scanning map. The distribution of Ti, O, P and Ni elements presents a hollow tubular shape, and P and Ni are uniformly distributed across the entire nanotube. Notably, a large number of obvious rod-like granular distribution patterns are not found on the inner wall of TiO_2 NTs. The possible reason is that the supply of precursor liquid in the tube hindered the growth of Ni_2P nanoparticles. Fig. S6 (f) is the EDS spectrum of Ni_2P/TiO_2-15, which shows that it is composed of Ti, O, P and Ni. Fig. S6 (g) shows the 400 nm long-line scan spectrum of the Ni_2P/TiO_2-15 nozzle. It can be observed from the figure that the distribution of Ti, O, P and Ni presents an increase in the protrusion content of the nozzle, and the closer to the center of the tube, the elements become less distributed.

The distribution of Ti and O indicates that TiO_2 has a hollow tubular structure with a certain thickness. The distribution characteristics of P and Ni indicate that Ni_2P is mainly distributed in the TiO_2 nanotube mouth, and its morphology also shows a hollow tubular structure, that is, its morphology is similar to the distribution of Ti and O but is not completely consistent. It can be observed that P and Ni protruding at the mouth of the tube is slightly offset, showing an irregular and messy distribution of rod-shaped Ni_2P nanoparticles at the mouth of the TiO_2 NTs instead of being completely covered in a planar shape. This is consistent with the phenomenon observed by SEM and high-resolution TEM.

Fig. S7 shows the single Ni_2P/TiO_2-15 nanotube and its line scan elemental mapping. As observed, P and Ni are evenly distributed on TiO_2 NTs in a semi-circular shape, consistent with the distribution state of Ti and O elements.

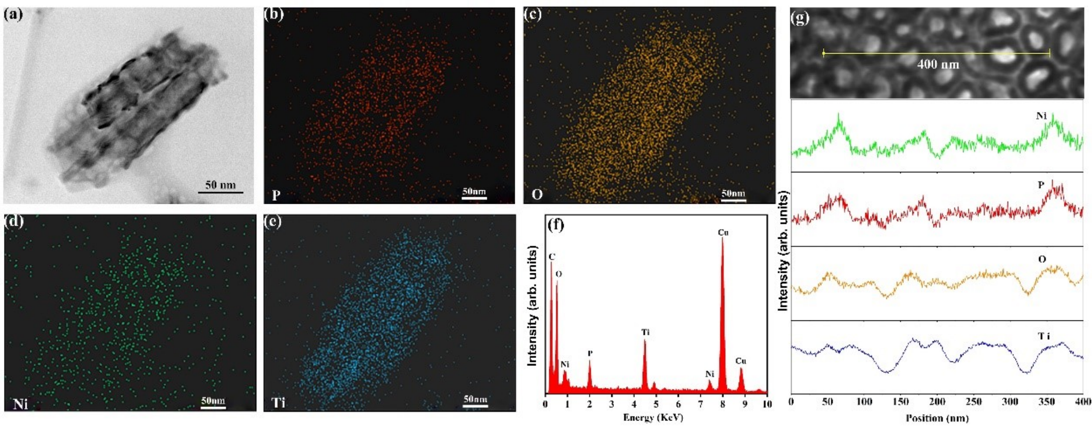

Fig. S6 (a-e) TEM image of Ni_2P/TiO_2-15 and its elemental mapping; (f) EDS images of Ni_2P/TiO_2-15;(g) line scan of the Ni_2P/TiO_2-15 nozzle

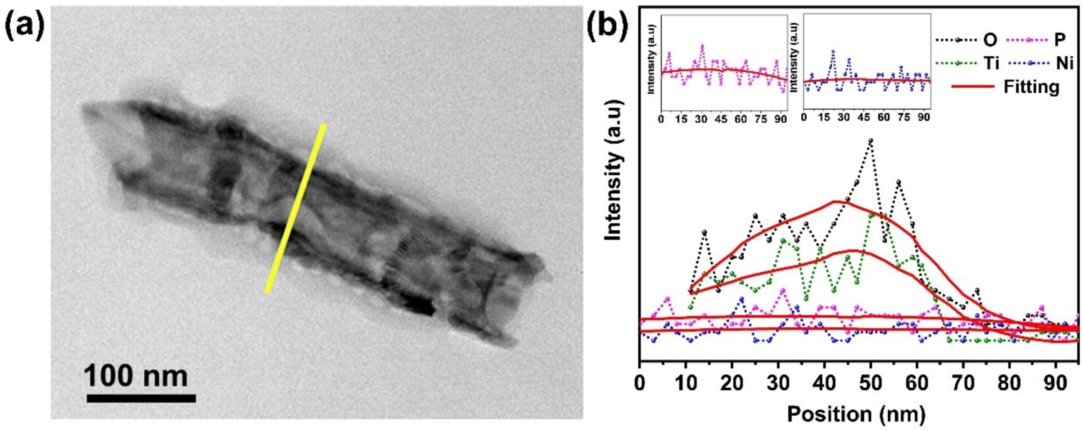

Fig. S7 (a) TEM image of single Ni_2P/TiO_2-15 nanotube and its line scan elemental mapping

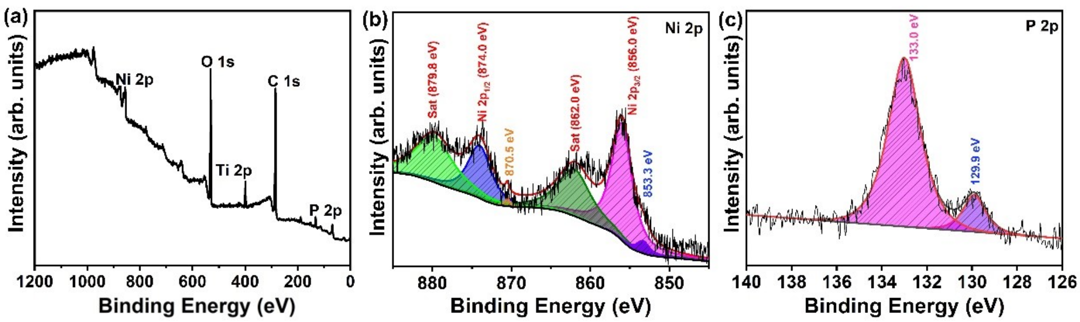

Fig. S8 XPS survey spectra of the Ni_2P/TiO_2-15 sample; (b-c) high-resolution XPS spectra of Ni 2p and P 2p of the Ni_2P/TiO_2-15 sample

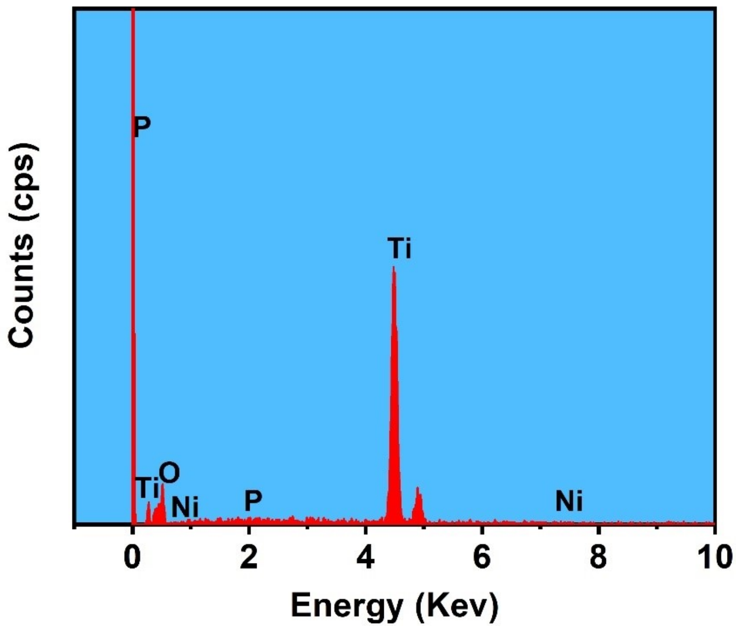

Fig. S9 EDS spectra of the Ni_2P/TiO_2-1 sample

Table S1 Atomic percentages of the elements in Ni_2P/TiO_2 composite

Samples	Atomic percentages, %			
	P	Ni	O	Ti
Ni_2P/TiO_2-1	0.2	0.5	39.4	59.9
Ni_2P/TiO_2-15	0.4	0.7	46.8	52.0
Ni_2P/TiO_2-30	0.4	0.9	29.6	69.1

Table S2. Parameter values of fitting decay curve and calculated values of carrier lifetime.

Samples	τ1	A1	τ2	A2	τ
TiO_2	1.42	858.47	13.36	140.31	8.65
Ni_2P/TiO_2-1	1.64	938.19	14.56	129.33	8.75
Ni_2P/TiO_2-15	2.55	1475.26	31.24	80.06	14.00
Ni_2P/TiO_2-30	1.46	885.31	14.88	128.37	9.46

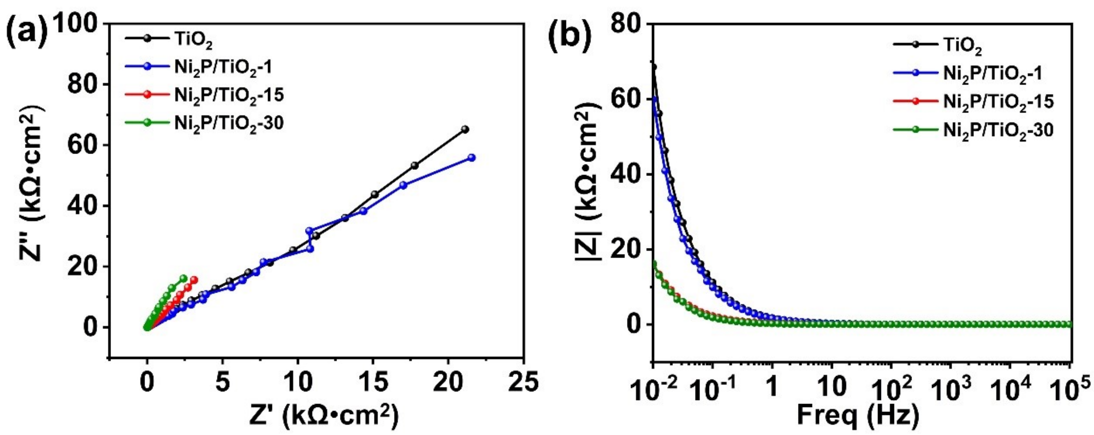

Fig. S10 (a) Nyquist plots of the TiO_2 NTs and Ni_2P/TiO_2 composites; (b) Bode plots of the TiO_2 NTs and Ni_2P/TiO_2 composites

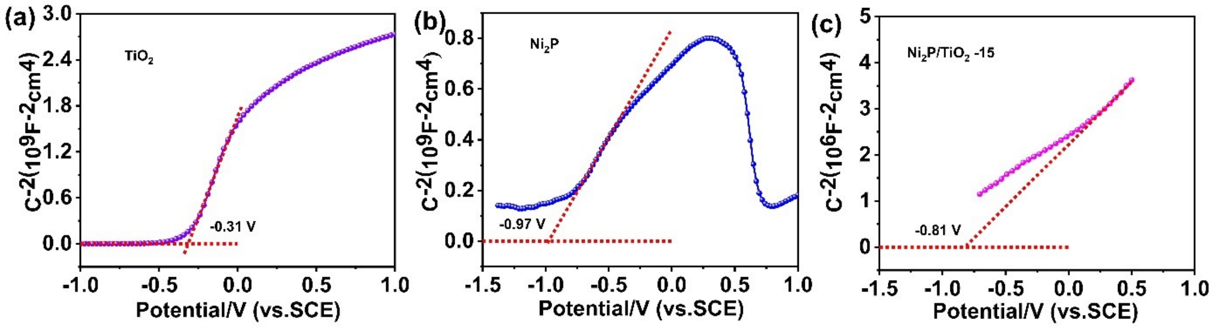

Fig. S11 Mott-Schottky plots of TiO_2 NTs, Ni_2P and Ni_2P/TiO_2 composites

Table S3 Work function value under vacuum environment and solvent effect.

Samples	Work function of vacuuming	Work function of solvation	ΔΦ
TiO_2 NTs	5.10	4.372	0.728
Ni_2P	3.46	3.712	-0.252
Ni_2P/TiO_2 composite	4.53	3.872	0.658

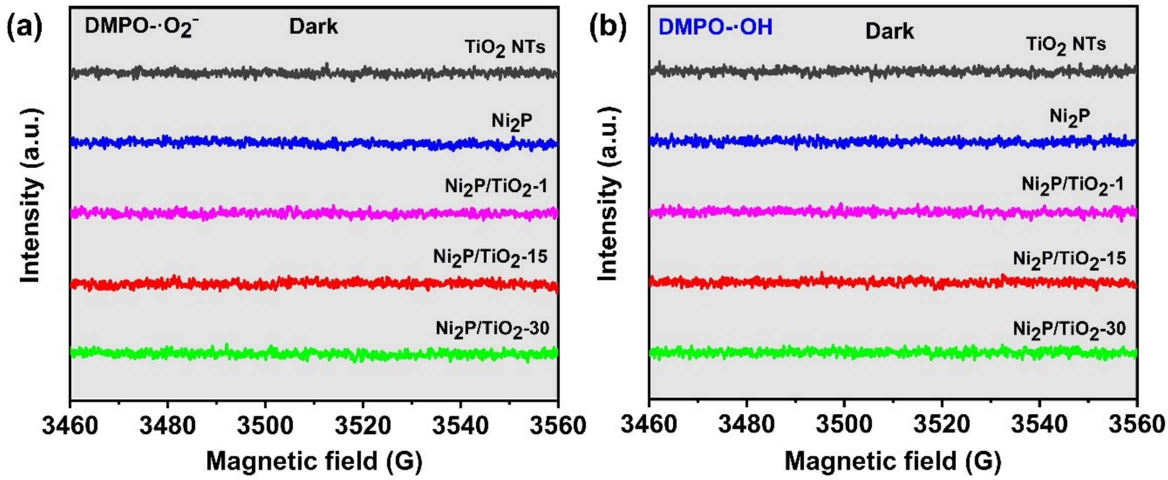

Fig. S12 (a) ESR spectra of TiO_2 NTs, Ni_2P and Ni_2P/ TiO_2 for DMPO-·O_2^- in dark; (b) ESR spectra of TiO_2 NTs, Ni_2P and Ni_2P/ TiO_2 for DMPO-·OH in dark

Table S4 OCP of the 304ss electrode coupled with the TiO_2 NTs and Ni_2P/TiO_2 composite photoanodes under illumination

Samples	TiO_2 NTs	Ni_2P/TiO_2-1	Ni_2P/TiO_2-15	Ni_2P/TiO_2-30
OCP (V)	-0.46	-0.75	-0.83	-0.78

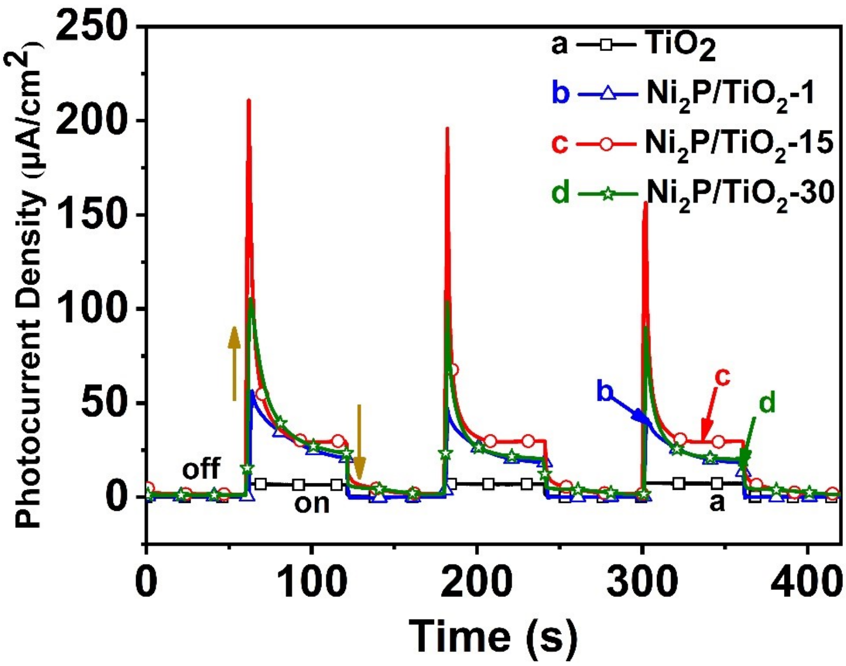

Fig. S 13 j-t curves of the 304ss electrode coupled with the TiO_2 NTs and Ni_2P/TiO_2 composite photoanodes under visible light

Table S5 j value of the 304ss electrode coupled with the TiO_2 and Ni_2P/TiO_2 composite photoanodes under illumination

Samples	TiO_2 NTs	Ni_2P/TiO_2-1	Ni_2P/TiO_2-15	Ni_2P/TiO_2-30
j ($\mu A/cm^2$)	6.9	55.2	209.4	104.6

Table S6 Performance comparison with reported articles.

Systems	**Strategy**	**Metal**	**Current density ($\mu A/cm^2$)**	**OCP (mV)**	**Stability/h**
This work	S-scheme	304ss	209.4	-830	50

MOF/TiO_2[6]	Type-II heterojunction	304ss	20.0	-730	48
$CuInS_2/TiO_2$[7]	Type-II heterojunction	316Lss	46.5	-860	/
PDA/TiO_2[8]	Type-II heterojunction	304ss	42.0	-780	15
$ZnWO_4/TiO_2$[9]	Type-II heterojunction	304ss	54.0	-780	/
Ni_3S_2 /TiO_2[10]	Type-II heterojunction	304ss	53.0	-720	/

The test electrolytes is 0.1 mol L-1 Na_2S and 0.2 mol L-1 NaOH solutions. Light source is visible light.

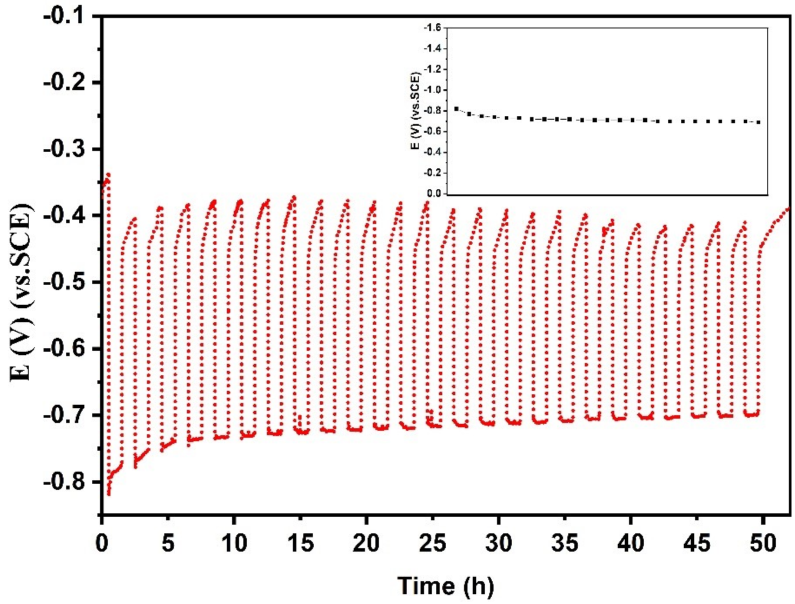

Fig. S14 OCP-t curves of 304ss coupled with the Ni_2P/TiO_2 composite photoanodes under visible light for 50 h (25 cycles), and the inset the value of the 304ss surface protected under light conditions

References

1. G. Kresse and J. Furthmüller, *Computational Materials Science*, 1996, **6**, 15-50.
2. G. Kresse and J. Furthmüller, *Physical Review B*, 1996, **54**, 11169-11186.
3. J. P. Perdew, K. Burke and M. Ernzerhof, *Physical Review Letters*, 1996, **77**, 3865-3868.
4. G. Kresse and D. Joubert, *Physical Review B*, 1999, **59**, 1758-1775.
5. P. E. Blöchl, *Physical Review B*, 1994, **50**, 17953-17979.
6. S. Guo, L. Chi, T. Zhao, Y. Nan, X. Sun, Y. Huang, B. Hou and X. Wang, *Journal of Electroanalytical Chemistry*, 2021, **880**.
7. W. Wang, Z. Yang, G. Li, Y. Zhang, W. Cao, J. Xu and R. Zheng, *J. Alloy. Compd.*, 2022, **890**.
8. J.-Y. Pu, X.-T. Wang, J.-Q. Liu, M.-P. Ren, Y.-B. Nan, M.-S. Liu, H. Xu, L.-H. Yang, Y.-L. Huang and B.-R. Hou, *Journal of Electroanalytical Chemistry*, 2022, **914**.
9. X. Wang, J. Lei, Q. Shao, X. Li, X. Ning, J. Shao, J. Duan and B. Hou, *Nanotechnology*, 2019, **30**, 045710.
10. Y. Nan, X. Wang, X. Ning, J. Lei, S. Guo, Y. Huang and J. Duan, *Surface and Coatings Technology*, 2019, **377**.